Journal of Power Sources, 51 (1994) 445–456

Destructive physical analysis results of Ni/H_2 cells cycled in low earth orbit regime (II)

Hong S. Lim and Gabriela R. Zelter
Industrial Electronics Group of Hughes Aircraft Company, Torrance, CA 90505 (USA)

John J. Smithrick
NASA Lewis Research Center, Cleveland, OH 44135 (USA)

Stephan W. Hall
Naval Weapons Support Center, Crane, IN 47522 (USA)

(Received December 14, 1993; accepted in revised form March 10, 1994)

Abstract

Six 48-Ah individual pressure vessel Ni/H_2 cells containing 26 and 31% KOH electrolytes have been on a low earth orbit cycle-life test. Three cells containing 31% KOH have failed after an average of 6400 cycles while the other three with 26% KOH have cycled for an average of 19 500 cycles. We have carried out post-cycle characterization tests and destructive physical analyses (DPA) of all cells. The DPA included visual inspections, measurements of electrode thickness, scanning electron microscopy, chemical analyses, and measurements of nickel electrode capacity in an electrolyte flooded cell. A gradual decrease of the usable cell capacity at high rate (1.4*C*) was the failure mode of all cells tested. Decrease of the usable capacity was due to decrease in the utilization of the active material with cycling mainly due to build-up of low rate capacity (residual capacity) and undischargeable active material. Cycle life of one of the cells might have been shortened prematurely due to the breakage of the cell core. Many gradual changes occurred with cycling at a rate which is independent of the KOH concentration. Each of these individual changes are difficult to be attributed to be the direct cause of the utilization decrease. However, an involved interaction of the changes might be responsible for the decrease.

Introduction

A dramatic improvement of cycle life of a Ni/H_2 cell has been demonstrated in boilerplate test cells [1, 2] by using 26% KOH electrolyte instead of conventional 31%. In order to confirm this improvement NASA Lewis Research Center has a contract with the Naval Weapons Support Center (NWSC) to test six 48-Ah Hughes recirculation design individual pressure vessel (IPV) Ni/H_2 flight cells [3, 4]. Three of these cells contain 26% KOH electrolyte and the other three contain 31% KOH. These cells have been tested under a low earth orbit (LEO) regime consisting of a 54-min charge followed by a 36-min discharge at 80% depth-of-discharge and 10 °C. Three cells containing 31% KOH electrolyte had an average cycle life of 6400 cycles (cell 1: 3729, cell 2: 4165 and cell 3: 11 355, respectively), while the average life of the other three cells containing 26% KOH electrolyte was 19 500 cycles (cell 4: 23 659,

Elsevier Science S.A.
SSDI 0378-7753(94)01923-J

cell 5: 15 314 and cell 6: 19 518, respectively). Results of cycling tests were described earlier [4–6]. Preliminary results of post-cycle characterization tests and destructive physical analyses (DPA) of three cells containing 31% KOH electrolyte were reported earlier [7]. The present report describes the results for all six cells containing 26 and 31% KOH electrolytes and discusses possible causes of the failure.

Experimental

Cell design

All cells were flight quality cells which were rated at 48 Ah and equipped with individual strain gauges. Cell stacks were made of 44 nickel electrodes in a recirculation stack design using zirconia separators. All cells had a nickel electrode precharge. Three of the cells were activated using 31% KOH electrolyte. The other three cells were activated using 26% KOH electrolyte.

Post-cycle characterization

Post-cycle characterization tests at NWSC included measurements of cell capacity by discharging cells at 24 A (C/2), 48 A (*C*), 67.2 A (1.4*C*) and 96 A (2*C*), respectively, to 1.0 V after charging them at 24 A for 2 h and then additional charging at 4.8 A (*C*/10 rate) for 6 h at 10 °C.

Pre-disassembly test at Hughes included additional capacity measurements in addition to a cell leak test, cell pressure measurement by strain gauge, and visual inspections. First cycle (conditioning cycle) involved charging cells at 4.8 A (*C*/10 rate) for 18 h followed by discharging them at 67.2 A (1.4*C*) to 1.0 V and further discharge at 4.8 A to 0.0 V at 10 °C. Second and third cycles (also at 10 °C) involved charging cells at 24 A for 2 h and then additional charging at 4.8 A for 6 h followed by discharging them at 67.2 A (1.4*C*) to 1.0 V and further discharge at 4.8 A to 0.0 V. The fourth cycle test was a 72-h open-circuit stand test at 20 °C after charging cells at 4.8 A for 10 h.

Disassembly analyses

All cells were shorted using a 1-Ω (5 W) resistor for a minimum of 16 h followed by a dead short for a minimum of 4 h prior to the disassembly. Disassembly analyses included visual inspections and photographing of the cell stacks and components, inspection of 'popping' damage of hydrogen electrodes, electrolyte analyses for KOH and carbonate after a Soxhlet extraction of a portion of the stack (five unit cells), electrode thickness measurements, flooded electrolyte capacity measurements of nickel electrodes with three different amounts of overcharge, chemical analyses of nickel electrodes, and scanning electron microscopy (SEM).

Flooded electrolyte capacity measurements were carried out in an electrolyte of the same KOH concentration as in the cell. Each cell included a pair of nickel electrodes from near top, middle and bottom of the original cell stack position. Three duplicate measurements were carried out after charging cells at 0.22 A for 16, 22 and 40 h, respectively, followed by discharging them at 1.10 A to −1.5 V versus a nickel sheet counter electrode.

Results and pre-disassembly characterizations

Capacities were measured at 1.4*C* rate to 1 V and residual capacities at *C*/10 rate to 0 V before and after the cycle-life test as shown in Fig. 1. The capacities to 1 V decreased by an average of 28% and 37% for cells containing 31% KOH and 26% KOH, respectively. The residual capacities of all cells increased drastically as shown in Fig. 1. Typical discharge voltage curves of cells containing 31 and 26% KOH electrolytes before and after the cycle-life test are compared with one another in Figs. 2 to 5. The discharge voltage of 31% KOH cells was depressed significantly after the cycle-life test as shown in Figs. 2 and 3. The voltage depression is more pronounced as the discharge rate increased. The discharge voltage of 26% KOH cells, however, did not change significantly after the cycle-life test as shown in Figs. 4 and 5. The voltage at a low rate (*C*/2) discharge is slightly improved instead of being depressed.

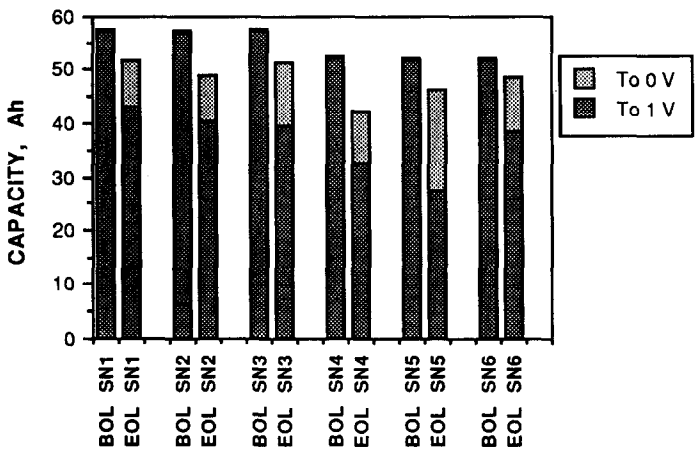

Fig. 1. Cell capacity measured at 1.4*C* rate discharge to 1.0 V and then *C*/10 rate discharge to 0.0 V (residual capacity). SN1 represents cell 1, SN2 cell 2 and so on. BOL: beginning-of-life, EOL: end-of-life.

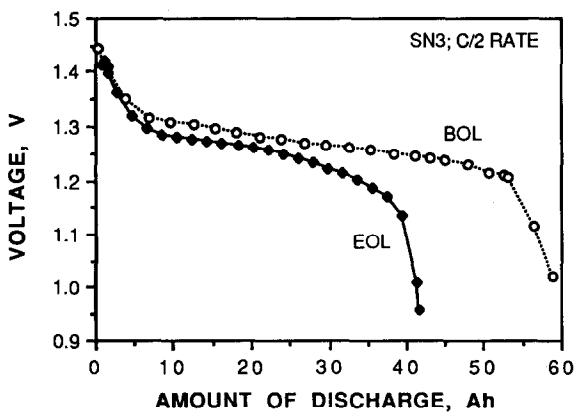

Fig. 2. Discharge voltage curves at *C*/2 discharge rate before (BOL) and after (EOL) the cycle-life test for cell 3 containing 31% kOH electrolyte.

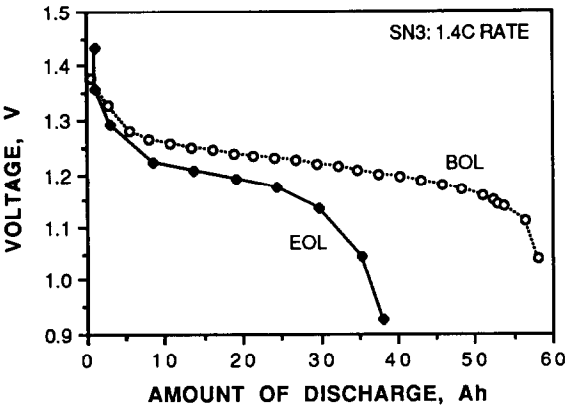

Fig. 3. Discharge voltage curves at 1.4*C* discharge rate before (BOL) and after (EOL) the cycle-life test for cell 3 containing 31% KOH electrolyte.

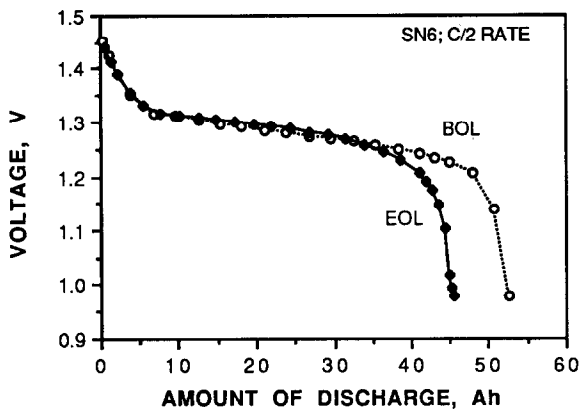

Fig. 4. Discharge voltage curves at *C*/2 discharge rate before (BOL) and after (EOL) the cycle-life test for cell 6 containing 26% KOH electrolyte.

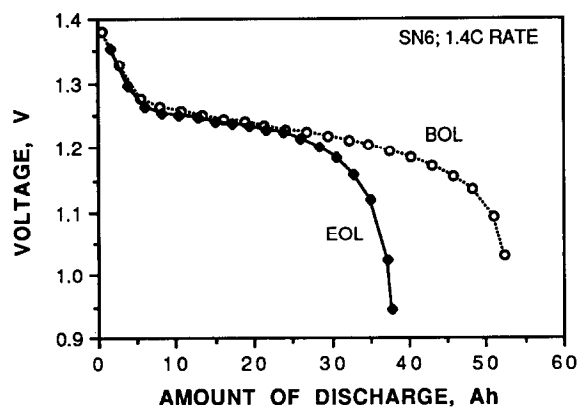

Fig. 5. Discharge voltage curves at 1.4*C* discharge rate before (BOL) and after (EOL) the cycle-life test for cell 6 containing 26% KOH electrolyte.

TABLE 1

Comparison of approximate self-discharge rates during 72-h charge retention test before and after the cycle-life test

	Total capacity at *C*/2 to 0 V at 10 °C (Ah)	72-h charge retention at 20°C (Ah)[a]	Self-discharge in 72 h (Ah)[b]	Average self-discharge rate (Ah/h)[b]
Cell1				
BOL[c]	59.17	35.08	24.09	0.33
EOL[c]	50.96	20.56	30.4	0.42
Cell 2				
BOL	58.88	35.11	23.77	0.33
EOL	48.78	21.18	27.6	0.38
Cell 3				
BOL	59.25	34.89	24.36	0.34
EOL	51.41	18.8	32.6	0.45
Cell 4				
BOL	53.50	34.47	19.03	0.26
EOL	43.92	0.00	>44	~1.5
Cell 5				
BOL	53.25	34.40	18.85	0.26
EOL	44.10	8.43	35.67	0.50
Cell 6				
BOL	52.94	34.35	18.59	0.26
EOL	45.50	8.61	36.89	0.51

[a]Measured after 10-h charge at *C*/10 rate.
[b]Values are approximate because the cycle regime for total capacity measurement and the state-of-charge at the beginning (see[a]) of the 72-h charge retention test are not the same. Values shown are worse than real ones.
[c]BOL: beginning-of-life; EOL: end-of-life.

Results of a charge retention test of the cells after a 10-h charge at *C*/10 rate followed by a 72-h open circuit at 20 °C are summarized in Table 1. Charge retention values were significantly reduced at the end-of-life (EOL) from those at the beginning-of-life (BOL) showing increase of self-discharge rate with cycling. The increase of self-discharge rate was higher for the 26% KOH cells than those for 31% KOH cells.

Results of disassembly analyses

All six cells showed no indication of leak or damage of cell case prior to the disassembly. Residual pressures in fully discharged state of cells were obtained from strain gauge readings immediately prior to the disassembly of the cells. The pressure increased linearly with cycling at a rate of 6.9 psi per 1000 cycles as shown in Fig. 6. This rate is approximately one third of that of the increase in end-of-charge pressure (EOCP) with cycling (21.2 psi per 1000 cycles) [5].

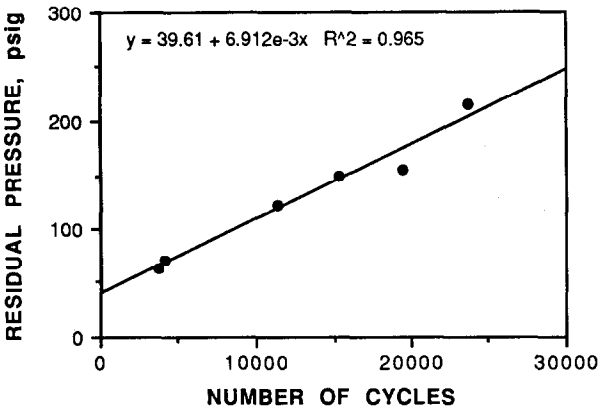

Fig. 6. Increase of residual pressure with cycling.

Visual inspections

All cell stacks looked dry without any excess electrolyte outside the stack. Outer appearances of all stacks were free of any visible damages. When the stacks were taken apart, cores (holding structure of the stack) of cell 4 and cell 5 were broken loose. These breakages caused the stack height to expand unevenly by 0.5 to 1.0 cm from initial height of ~9.0 cm. All nickel electrodes showed some degree of gas screen imprints indicating that there was extrusion of active material from inside of the electrode to outside. The degree of the extrusion generally increased from top (positive terminal side) to the bottom (negative terminal). The cause of the variation of the extrusion appears to be gravitational segregation of the electrolyte making the bottom part wetter than the top part. Similar extrusion and its variations were also observed with nickel electrodes from heavily cycled cells [2, 7, 8]. There were indications of localized hydrogen/oxygen recombinations (popping) on the hydrogen electrodes which are commonly observed from cycled cells of a similar design. Visible variation of the popping from one cell to another was rather minimal. In summary, there was no apparent visible sign of an abnormal failure with exception of the core breakage which is a suspected cause of the premature failure of cell 5.

Electrode thickness change

Thickness of the cycled electrodes were measured at three different locations on each electrode using a micrometer. The values of electrode expansion depended on the electrode positions in the stack. The expansion was heavier at the bottom of the stacks than at the top, especially for those cycled heavily, as shown in Fig. 7. The reason for heavier expansion at the bottom is speculated as follows. The electrode at lower positions had larger amount of electrolyte (wetter) than those at higher positions (drier) due to gravitational segregation of the electrolyte. Therefore, the unit cells at lower positions had lower internal resistance and cycled more heavily than those at higher positions. Average values of the expansion are shown against number of cycles in Fig. 8.

Scanning electron microscopy

Scanning electron microscopy (SEM) pictures of various magnifications ($\times 100$ to $\times 500$) of electrode surface, fractured surface and metallographic cross sections of nickel electrodes were studied. Typical changes of the electrodes are shown in Fig.

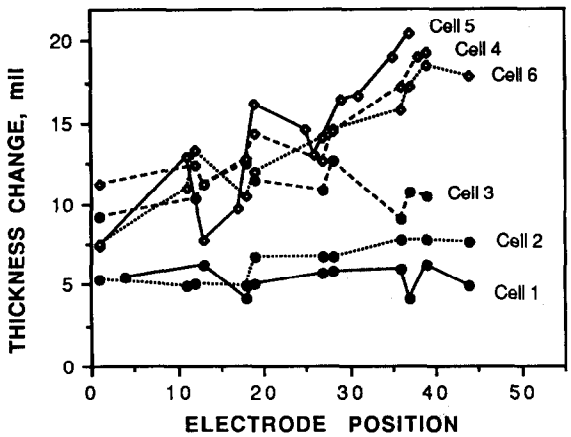

Fig. 7. The expansion of nickel electrodes as a function of the vertical positions in the cell stack; mil = 0.0254 mm.

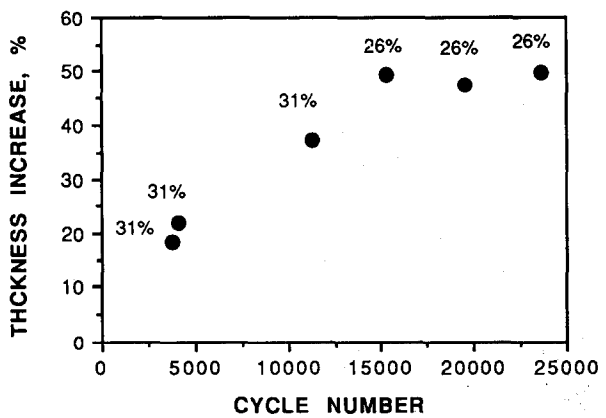

Fig. 8. Average expansion of nickel electrodes vs. number of cycles. Data points represent an average value from each cell.

9(a) for relatively low number of cycles (cell 2) and in Fig. 9(b) for high number of cycles (cell 6). These SEM pictures show dimensional expansion of the electrode, active material extrusion and damages (fracture) of sinter structure by the expansion. The general feature and characteristics of these changes are similar to those observed previously [2, 8]. Although there is an obvious increase in damages as the number of cycles increases, the degree of the damage was not quantitatively related to capacity losses of the electrode as shown in the 'Electrochemical utilization of electrodes' section later.

Chemical analyses

Chemical analyses were carried out on the electrolyte and six nickel electrodes which were used for electrode capacity measurements in flooded electrolyte cells. Results of electrolyte analyses showed that concentrations of total potassium ion and K_2CO_3 increased linearly with cycling as shown in Figs. 10 and 11, respectively. The

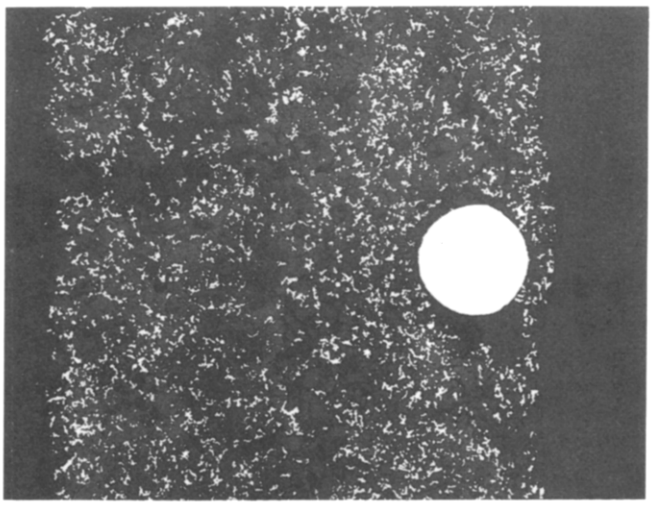

(a)

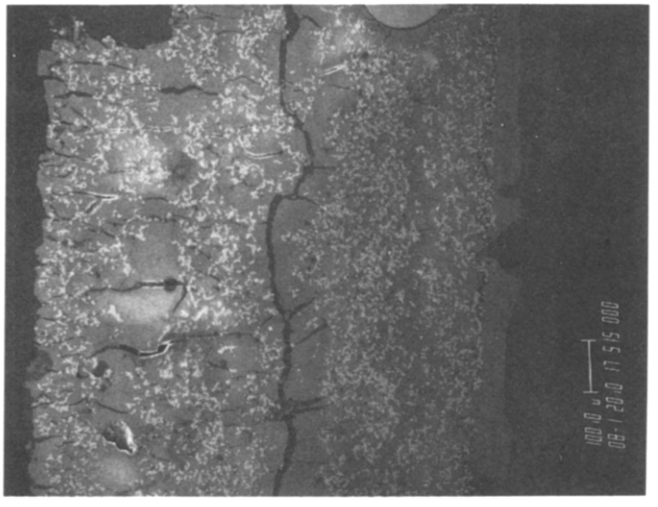

(b)

Fig. 9. SEM pictures (approximately $\times 100$) of the cross-sectional area of a nickel electrode from cell 2 (a) and cell 6 (b).

increase of total potassium ion concentration is due to the fact that water is consumed by corrosion reaction of the plaque. The source of K_2CO_3 might be the oxidation of carbon impurity in the carbonyl nickel powder of the plaque.

Theoretical capacities of cell calculated from total ionic active material (Ni and Co) are plotted against number of cycles in Fig. 12. The capacity increased linearly with cycling. This capacity increase is probably due to production of nickel hydroxide/oxide active material as the reaction product of the corrosion. Cobalt content in the active material decreased slowly with cycling as shown in Fig. 13 as expected by dilution due to the increase of the nickel hydroxide/oxide by corrosion. Total amount of the

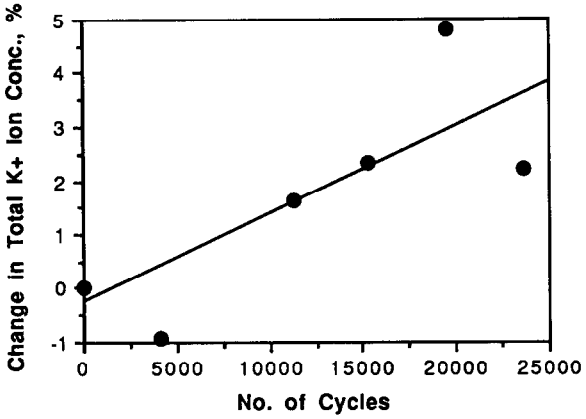

Fig. 10. Changes in total potassium concentrations are shown vs. number of cycles.

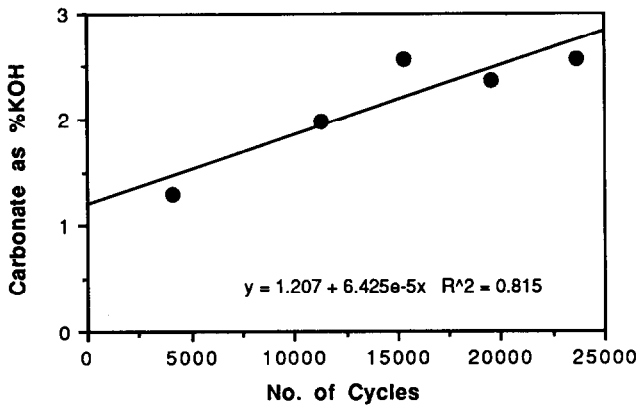

Fig. 11. Increase of K_2CO_3 concentrations are shown vs. number of cycles.

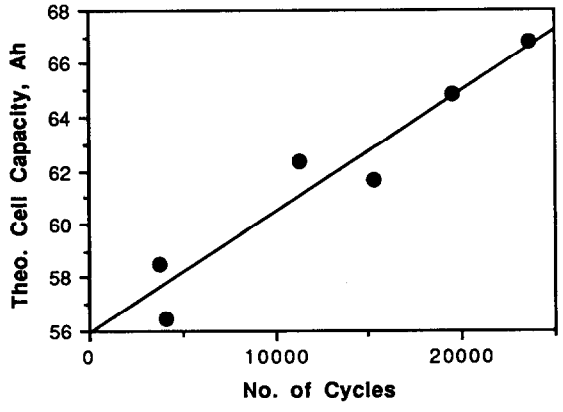

Fig. 12. Increase of theoretical cell capacity calculated from total ionic active material by chemical analysis vs. number of cycles.

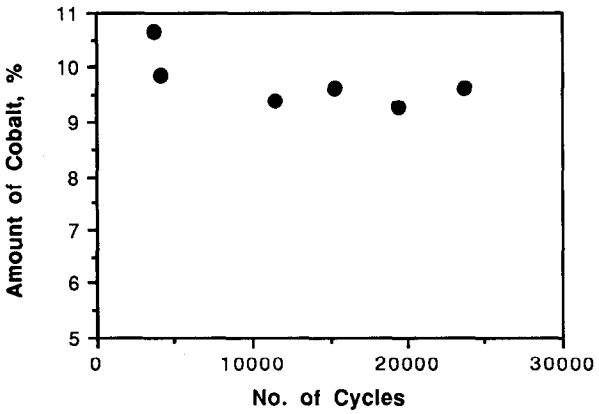

Fig. 13. Cobalt content in the active material vs. number of cycles.

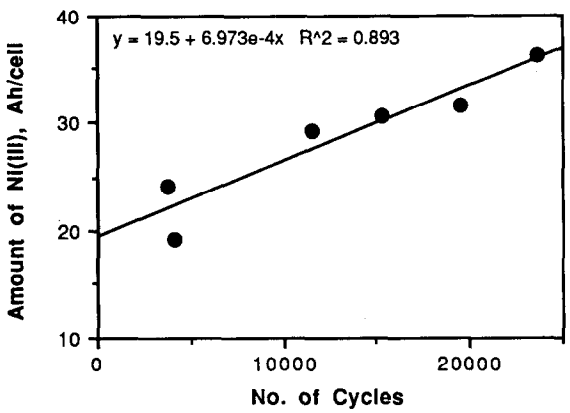

Fig. 14. Amount of ionic nickel and cobalt in oxidation state (III) (abbreviated as Ni(III)) in the cell vs. number of cycles.

active material in the cell in oxidation state (III) was plotted against number of cycles in Fig. 14. This amount increased linearly with cycling in an average rate of 0.7 mAh per cycle indicating that electrochemically undischargeable active material is accumulated with cycling.

Electrochemical utilization of electrodes

Electrochemical utilization of active material was evaluated from the amount of total active material determined by chemical analysis and electrode capacity values measured in the electrolyte flooded cells after *C*/10 rate charging for 16, 22 and 40 h, respectively. The utilization values based on the 16-h capacity are plotted against number of cycles in Fig. 15. The cell average values of the utilization of the cycled electrodes were all within $71 \pm 3\%$. However, the data spread for three cells (pair of electrodes) were quite variable as shown in Fig. 15.

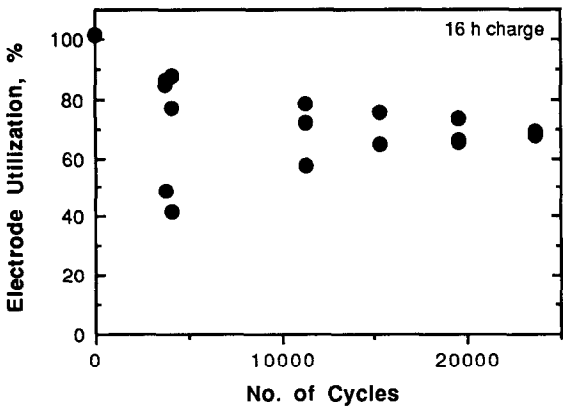

Fig. 15. Nickel electrode capacity values in a flooded electrolyte cell by discharging at *C*/2 rate to −1.5 V vs. a nickel sheet counter electrode after charging for 16 h at *C*/10 rate. Each data point represents an average utilization of a pair of nickel electrodes.

Discussion

Cycle-test results show that all cells failed due to a gradual decrease of the usuable cell capacity at high rate (1.4*C*) with cycling rather than an abrupt failure. Decrease in overall electrochemical capacity including low rate capacity (residual capacity) was relatively small, see Fig. 1. There was no catastrophic damage in the stack structure. A possible exception, however, may be the breakage of the cell cores of cell 4 and cell 5 which might have shortened their cycle life, especially cell 5. The gradual cell capacity decrease was due to the decrease of the utilization of active material by approximately 30% during the course of life. Although an individual change alone is difficult to be attributed to be the cause of the utilization decrease, a number of changes, which might be partially responsible for the decrease, were observed as discussed below:

(i) The electrode expanded significantly (Figs. 7 and 8), although the expansion is not quantitatively related to the capacity decrease.

(ii) Sintered substrate was ruptured as the electrode expanded (Fig. 9). However, the extent of such rupture is apparently not quantitatively related to the capacity decrease.

(iii) Total concentration of the potassium ion was increased indicating that the amount of water and therefore electrolyte in the cell was reduced (Fig. 10).

(iv) Concentration of K_2CO_3 was increased with cycling (Fig. 11). However, the increase is not quantitatively related to the capacity decrease.

(v) Plaque substrate was corroded with cycling. However, the amount of corrosion is not quantitatively related to the capacity decrease.

(vi) The cobalt concentration in the active material decreased with cycling (Fig. 13). However, the decrease is difficult to relate quantitatively to the capacity decrease.

(vii) The amount of undischargeable active material in oxidation state (III), or higher, increased with cycling (Fig. 14). However, this amount is not quantitatively related to the capacity decrease, either.

In summary, although it is difficult to single out a specific change which is responsible for the capacity decrease, we have measured many changes which probably cause the capacity decrease through loss of rate capability (build-up of the residual

capacity as shown in Fig. 1) and build-up of the electrochemically undischargeable active material (Fig. 14).

The rates of the most of changes described above are indistinguishable between the two different concentrations of KOH (26 and 31%). These changes include the electrode expansion (Fig. 8), total concentration of the potassium ion (Fig. 10), concentration of K_2CO_3 (Fig. 11), rate of corrosion (Fig. 12) and the amount of undischargeable active material (Fig. 14). Even though the rates of these changes are comparable, the cycle life of 26% KOH cells was three times longer than those of 31% KOH cells indicating that the nickel electrodes can take three times more such changes in the 26% KOH electrolyte than in the 31% KOH electrolyte before their performance suffered.

Conclusions

1. A gradual decrease of the usable cell capacity at high rate (1.4*C*) was the failure mode of all cells tested.
2. Decrease of the usable capacity was due to decrease in the utilization of the active material with cycling mainly due to build-up of low rate capacity (residual capacity) and undischargeable active material.
3. Cycle life of one of the cells (cell 5) might have been shortened prematurely due to the breakage of the cell core.
4. Many changes occurred linearly with cycling at a rate which is independent of the KOH concentrations. Each of these individual changes are difficult to be attributed to be the direct cause of the utilization decrease. However, an involved interaction of the changes might be responsible for the decrease.

Acknowledgement

This work is supported by a NASA Lewis Research Center (Contract No. NAS 3-22238).

References

1 H.S. Lim and S.A. Verzwyvelt, *J. Power Sources, 22* (1988) 213.
2 H.S. Lim and S.A. Verzwyvelt, *J. Power Sources, 29* (1990) 503.
3 J.J. Smithrick and S.W. Hall, *Proc. 25th Intersociety Energy Conversion Engineering Conf., Aug. 1990, Reno, NV, USA,* Vol. 3, p. 16.
4 J.J. Smithrick and S.W. Hall, *Proc. 26th Intersociety Energy Conversion Engineering Conf., Boston, MA, USA, Aug. 1991,* Vol. 3, p. 276.
5 H.S. Lim and J.J. Smithrick, *Proc. 28th Intersociety Energy Conversion Engineering Conf., Atlanta, GA, USA, Aug. 1993,* Vol. 1, p. 151.
6 J.J. Smithrick and S.W. Hall, *Proc. 27th Intersociety Energy Conversion Engineering Conf., San Diego, CA, USA, Aug. 1992,* Vol. 1, p. 215.
7 H.S. Lim, G.R. Zelter, J.J. Smithrick and S.W. Hall, *Proc. 26th Intersociety Energy Conversion Engineering Conf., Boston, MA, USA, Aug. 1991,* Vol. 3, p. 304.
8 H.S. Lim and S.A. Verzwyvelt, *Proc. 19th Intersociety Energy Conversion Engineering Conf., San Francisco, CA, USA, Aug. 1984,* p. 312.